J Mater Sci (2010) 45:6365–6373
DOI 10.1007/s10853-010-4623-0

IMEC 2009

# The influence of the cooling rate on bulk metallic glass formation in $Mg_{80}Cu_{15}Y_5$ and $Mg_{80}Cu_{10}Y_{10}$

**M. Regev · H. Rosenson · Z. Koren · A. Katz-Demyanetz**

Received: 22 November 2009 / Accepted: 14 May 2010 / Published online: 25 May 2010


**Abstract** The Mg–Cu–Y system is known to be one of the best glass formers among the various existing magnesium alloys. The compositions chosen for the current study were $Mg_{80}Cu_{15}Y_5$ and $Mg_{80}Cu_{10}Y_{10}$. Different casting processes yielded four different microstructures that were analyzed by means of X-ray diffraction, scanning electron microscopy, high resolution scanning electron microscopy, and energy-dispersive X-ray spectroscopy chemical analysis. The different casting procedures were gravity castings of 3 mm diameter specimens into a copper mold held at different temperatures (cooled to −195 °C with the aid of liquid nitrogen, held at room temperature and heated up to 300 °C) and melt-spinning. Detailed microstructure study was then performed on the melt-spun specimen using transmission electron microscopy and high resolution transmission electron microscopy. The above-mentioned investigation revealed a crystalline rather than amorphous structure. The observed microstructure could not be explained on the basis of current models referring to the frequency of nucleation events.

## Introduction

Magnesium alloys are attractive for engineering applications such as the automotive industry due to their good physical properties, namely, high strength, light weight, good damping absorption, and good thermal and electrical conductivity. Furthermore, amorphous magnesium alloys exhibit higher strength, hardness and a large elastic domain in addition to excellent corrosion resistance [1–6]. Among the various existing magnesium alloys, the Mg–Cu–Y system is known to be one of the best glass formers [5]. The growing interest in high glass forming abilities (GFAs) has led to the formulation of semi-empirical rules that must characterize manufactured bulk metallic glass (BMG): (1) the presence of multicomponent systems (the confusion principle); (2) a significant difference in atomic size, above 12%, among the main constituent elements; (3) the occurrence of large negative mixing enthalpy; and (4) compositions close to deep eutectics [4, 7]. Below is a short summary of the research reported in the literature dealing with the microstructure of amorphous Mg–Cu–Y alloys.

Hong et al. [1] prepared $Mg_{60}Cu_{30}Y_{10}$ powders by the droplet emulsion technique (DET). By controlling the powder size they achieved undercooling of 60–140 K. The microstructure obtained changed with the degree of undercooling, from lamellar eutectic to dendritic, to cellular, and finally, to a glassy phase.

Pryds et al. [5] obtained amorphous $Mg_{60}Cu_{30}Y_{10}$ by quenching the melt in a plate-shape copper mold. They studied the crystallization kinetics of the amorphous alloy by means of differential scanning calorimetry (DSC) but did not describe its microstructure.

Savyak et al. [6] prepared $Mg_{65}Cu_{25}Y_{10}$ glassy ribbons by melt spinning, their transmission electron microscopy study revealed an amorphous matrix phase with a few embedded nanocrystals 5–15 nm in size.

Satta et al. [7] investigated two different compositions, $Mg_{27}Cu_{38}Y_{35}$ and $Mg_{65}Cu_{25}Y_{10}$, prepared by a melt spinning technique. They found that the $Mg_{27}Cu_{38}Y_{35}$

M. Regev (✉)
Mechanical Engineering Department, Ort Braude College of Engineering, P.O. Box 78, Karmiel 21982, Israel
e-mail: michaelr@braude.ac.il

H. Rosenson · Z. Koren · A. Katz-Demyanetz
Foundry Laboratory, Israel Institute of Metals, Technion-Israel Institute of Technology, Technion City, Haifa 32000, Israel

composition, which did not approach the glass forming range, did not show amorphization under rapid solidification whereas full amorphization was obtained in the case of $Mg_{65}Cu_{25}Y_{10}$.

Inoue and Masumoto [8] and Inoue et al. [9] pointed out the maximum diameters for the formation of an amorphous single phase for $Mg_{90-x}Cu_xY_{10}$ produced by high pressure die casting. They found that the maximum diameter varies from 3 mm for a Cu content of 10 at.% up to 7 mm for a Cu content of 25 at.%. After performing tension tests on an amorphous $Mg_{80}Cu_{10}Y_{10}$ high pressure die cast specimen, they found that the fracture stress at room temperature (RT) is 630 MPa without appreciable elongation. DSC study of $Mg_{65}Cu_{25}Y_{10}$ showed that there was no appreciable difference in the glass transition temperature ($T_g$) and the onset temperature of crystallization ($T_x$) values between the cast and melt-spun samples [9]. In another study, Inoue et al. [10] compared $T_g$ and $T_x$ values of an Mg–Cu–Y metallic mold casting to those of a 0.02 mm thickness melt-spun ribbon and came to the same conclusion; namely, they saw that there was no appreciable difference in the values of $T_g$ and $T_x$ between the two processes. The critical diameter for the formation of an amorphous phase in the case of metallic mold casting was in the range of 1.0–4.0 mm in the composition range of 10–35 at.% Cu and 10–20 at.% Y and reached the maximum value for $Mg_{65}Cu_{25}Y_{10}$.

Wolff et al. [11] prepared bulk amorphous $Mg_{60}Cu_{30}Y_{10}$ alloys by rapid quenching in a copper mold. They found that controlled annealing of these specimens at 174 °C for different periods led to various degrees of partial crystallization, namely 15, 50, 75, and 100 vol.%. X-ray diffraction (XRD) and transmission electron microscope (TEM) studies of the microstructure revealed only a crystalline $Mg_2Cu$ orthorhombic phase. No equilibrium Mg–Y phase such as $Mg_{24}Y_5$ or $Mg_2Y$ was detected. The average grain size of the crystalline phase was about 100 nm; the nanocrystallized specimens showed an increase in the yield stress provided that their crystalline volume fraction was less than 50%. Larger volume fractions of nanocrystals promoted brittle fracture and reduced strength.

Chen and Ferry [12] studied the crystallization behavior of $Mg_{65}Cu_{25}Y_{10}$ BMG produced by mold casting by exposing it to 210, 230, and 250 °C for 3, 6, and 9 min, respectively They used XRD, DSC, and scanning electron microscopy for their investigation and found that the fully amorphous phase transforms into an amorphous phase containing $Mg_2Cu$ and, finally, into an Mg solid solution containing $Mg_2Cu$, $Mg_{24}Y_5$ and $Cu_2Y$.

Kim et al. [13] used XRD and TEM to study the compositional range in which an amorphous phase in the Mg–Cu–Y system is formed by melt spinning. They claimed that both compositions, $Mg_{80}Cu_{10}Y_{10}$ and $Mg_{80}Cu_{15}Y_5$, yield an amorphous phase under rapid cooling rates. The value they found for $\Delta T_x$ ($=T_g - T_x$) was about 20 K for both compositions.

Murty and Hono [14] studied the microstructure of melt-spun $Mg_{65}Cu_{25}Y_{10}$, $Mg_{80}Cu_{10}Y_{10}$, and $Mg_{80}Cu_{15}Y_5$ using TEM, XRD, and DSC. They concluded that nanodispersions of $Mg_2Cu$, hcp-Mg, and fcc-Mg with particle sizes of 5–20 nm were observed within the amorphous matrix of the $Mg_{65}Cu_{25}Y_{10}$, $Mg_{80}Cu_{10}Y_{10}$, and $Mg_{80}Cu_{15}Y_5$ alloys, respectively.

Using DSC and XRD, Ma et al. [15] showed that the optimal Mg–Cu–Y BMG formers are close to but do not quite match the eutectic composition. They showed that relatively small composition differences can result in doubling of the critical size for BMG formation compared to the critical size for eutectic composition.

Most investigators have studied compositions with relatively low Mg content (less than 65 at.%). In such cases obtaining a high GFA is mainly due to the presence of elements with significantly different atomic radii (Rules 1 and 2 mentioned above). To the best of the authors' knowledge, a study of the influence of the cooling rate on the microstructure together with a detailed microstructure analysis of the compositions having a magnesium content of 80 at.% is still lacking. Such a study on $Mg_{80}Cu_{15}Y_5$ was recently published by the authors [16] of the present paper. The current paper summarizes a similar investigation conducted on $Mg_{80}Cu_{10}Y_{10}$ and reveals characteristics of the Mg–Cu–Y system and its GFA by comparing the differences between results obtained for $Mg_{80}Cu_{10}Y_{10}$ and those obtained for $Mg_{80}Cu_{15}Y_5$.

## Experimental

The two chemical compositions studied were, as mentioned above, $Mg_{80}Cu_{15}Y_5$ and $Mg_{80}Cu_{10}Y_{10}$. Pure Mg and Cu metals and an Mg–40 wt% Y master alloy were used for the alloy preparation. Alloying was performed in a graphite crucible under an Ar protective atmosphere. The materials blend was melted and then homogenized at 750 °C for 1 h before casting. The alloy was then gravity-cast into a steel mold and air-cooled to RT. Gravity casting of 3 mm diameter specimens into a copper mold held at different temperatures (cooled to −195 °C with the aid of liquid nitrogen, held at RT and heated to 300 °C) and melt spinning were used in order to test various cooling rates. The details of the casting experiments are listed in Table 1. In all cases of gravity casting the temperature of the melt was measured by using a K type thermocouple; hence cooling rates could be calculated. For process no. 1 the cooling rate was found to be around 1 °C $s^{-1}$; in the case of the mold held at RT the cooling rate was found to be

**Table 1** Casting experiments

| No. | Casting process | Details |
|---|---|---|
| 1 | Permanent Cu mold | Mold held at 300 °C |
| 2 | Permanent Cu mold | Mold held at RT |
| 3 | Permanent Cu mold | Mold held at −195 °C |
| 4 | Melt spinning | Wheel rotation—1000 rpm, Ar atmosphere |

about 10 °C $s^{-1}$; and in the case of the mold held at −195 °C the cooling rate was found to be about 100 °C $s^{-1}$. As for the melt spinning process, the cooling rate was estimated to be about 1000000 °C $s^{-1}$. This estimation is based on both the literature [17] and a heat transfer calculation taking the thickness of the specimen and the geometry of the machine into account.

XRD tests were performed using a Philips-PW-1820 Bragg–Brentano geometry equipped with a Cu tube ($\lambda_{K\alpha} = 1.5406$ Å). The melt-spun specimen was ground to powder prior to the XRD tests in order to eliminate any texture influence. The microstructure was studied under a 20 kV Philips XL30 SEM equipped with an Oxford energy-dispersive X-ray spectroscopy (EDS) system and with a 10 kV FEI Quanta 200 scanning electron microscope (SEM). The fracture surface of the melt-spun specimens was studied with a 5 kV Leo-982 high resolution scanning electron microscope (HRSEM). TEM investigation was conducted using an FEI Tecnai T20 200 kV TEM and an FEI Titan 300 kV high resolution transmission electron microscope (HRTEM).

TEM specimens were prepared as follows:

1. 80 μm thick slices were cut from the melt-spun film.
2. The slices were ion milled using a Gatan-600 laser-terminated dual ion miller with an acceleration voltage of 5 kV and a current of 5 mA. The initial milling angle was 25°, which was then changed to 10°. The specimens were continually cooled with the aid of liquid nitrogen in order to avoid artifacts resulting from specimen heating.

## Results

XRD spectra of specimens cast by the four processes listed in Table 1 are given in Fig. 1. The numbering of the casting processes is identical to the numbering of Table 1, Fig. 1a refers to $Mg_{80}Cu_{15}Y_5$ and Fig. 1b refers to $Mg_{80}Cu_{10}Y_{10}$. The phases identified are Mg and $Mg_2Cu$; their peaks are shown in Fig. 1. It can be seen from Fig. 1a that only pattern no. 4 obtained from the $Mg_{80}Cu_{15}Y_5$ melt-spun specimen may be characterized as an amorphous one. In the case of the melt-spun $Mg_{80}Cu_{10}Y_{10}$ specimen, it may be claimed that the spectrum profile is close to that of an amorphous material (halo profile) together with clearly distinguishable broadened crystalline reflections peaks. The examined material seems to be, therefore, partially amorphous and partially crystalline.

Secondary electron SEM micrographs of the permanent Cu mold castings, held at 300 °C, are shown in Fig. 2. Figure 2a refers to $Mg_{80}Cu_{15}Y_5$, Fig. 2b refers to $Mg_{80}Cu_{10}Y_{10}$, and Fig. 2c is a backscattered electron (BSE) micrograph of the $Mg_{80}Cu_{10}Y_{10}$ specimen taken from the same region and under the same magnification as Fig. 2b. The microstructure is characterized by an acicular morphology that seems to be finer in the case of $Mg_{80}Cu_{10}Y_{10}$. Dark regions are discernible within the acicular structure. These regions are finer in the case of $Mg_{80}Cu_{10}Y_{10}$. Shiny bright particles having an average size of about 1 μm are scattered throughout both specimens. EDS analysis showed that the bright particles contain a high concentration of Y, about 60 at.% in the case of $Mg_{80}Cu_{15}Y_5$ and above 85 at.% in the case of $Mg_{80}Cu_{10}Y_{10}$. The chemical composition of the acicular structure was close to 80 at.% Mg and 20 at.% Cu for both $Mg_{80}Cu_{15}Y_5$ and $Mg_{80}Cu_{10}Y_{10}$. This acicular structure contains between 5 and 10 at.% Y. The dark regions mentioned above were found to be Mg with about 4 at.% Cu and 3 at.% Y in the case of $Mg_{80}Cu_{15}Y_5$. Unfortunately, no reliable EDS analysis could be performed on

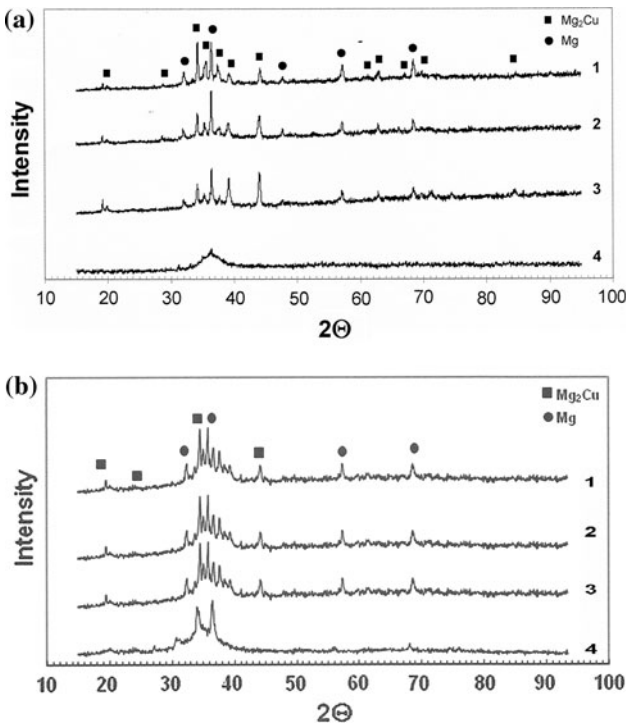


**Fig. 1** XRD patterns under various casting conditions and processes of **a** Mg80Cu15Y5 and **b** of $Mg_{80}Cu_{10}Y_{10}$

these dark $Mg_{80}Cu_{10}Y_{10}$ regions due to their fineness. However, the BSE micrograph given in Fig. 2c indicates a higher magnesium content within these dark regions.

SEM micrographs of the permanent Cu mold castings, held at −195 °C, are shown in Fig. 3. Figure 3a refers to $Mg_{80}Cu_{15}Y_5$, Fig. 3b refers to $Mg_{80}Cu_{10}Y_{10}$, and Fig. 3c is a BSE micrograph of the $Mg_{80}Cu_{10}Y_{10}$ specimen taken from the same region and under the same magnification as Fig. 3b. A few phases can be detected in this micrograph: a dark one, an acicular one and bright particles. EDS analysis showed that the chemical composition of the acicular phase is close to 80 at.% Mg and 20 at.% Cu in the case of $Mg_{80}Cu_{15}Y_5$ and close to 70 at.% Mg and 20 at.% Cu in the case of $Mg_{80}Cu_{10}Y_{10}$. This acicular phase contains between 5 and 10 at.% Y whereas a higher Y content was recorded for $Mg_{80}Cu_{10}Y_{10}$. The bright particles contain a high concentration of Y, as was shown in Fig. 2. The dark $Mg_{80}Cu_{15}Y_5$ regions were found to be Mg with about 4 at.% Cu and about 1 at.% Y. No reliable EDS analysis could be made on the dark regions in the case of $Mg_{80}Cu_{10}Y_{10}$ due to their fineness. However, the BSE micrograph shown in Fig. 3c indicates higher magnesium content within these dark regions.

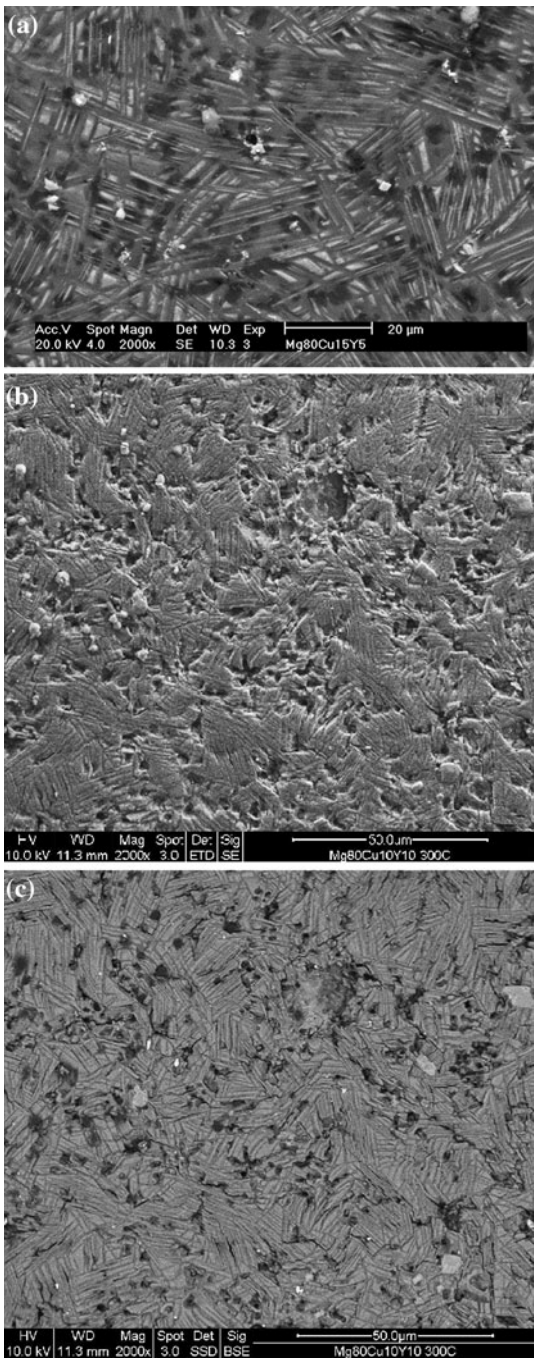


**Fig. 2** SEM micrograph of the gravity casting, mold held at 300 °C: **a** $Mg_{80}Cu_{15}Y_5$ SE, **b** $Mg_{80}Cu_{10}Y_{10}$ SE, **c** $Mg_{80}Cu_{10}Y_{10}$ BSE

SEM micrographs of the permanent Cu mold castings, held at −195 °C, are shown in Fig. 4. The microstructure is composed of a fine acicular structure containing dark particles. EDS analysis showed that the chemical composition of the acicular phase is close to 80 at.% Mg, 20 at.% Cu and about 5 at.% Y for both compositions. The bright particles are characterized, as in all other cases, by a Y concentration of more than 50 at.%. The dark phase in the case of $Mg_{80}Cu_{15}Y_5$ is Mg with about 9 at.% of Cu and about 2 at.% of Y. No quantitative EDS analysis of the dark phase in the case of $Mg_{80}Cu_{15}Y_5$ could be made due to its fineness but the BSE micrograph shown in Fig. 4c indicates higher magnesium content within these dark regions.

HRSEM micrographs of the specimens cast by the melt spinning process are shown in Fig. 5. Figure 5a refers to $Mg_{80}Cu_{15}Y_5$ and Fig. 5b refers to $Mg_{80}Cu_{10}Y_{10}$. It can be seen that the microstructure consists of spheres. In the case of $Mg_{80}Cu_{15}Y_5$ the size of these spheres is a few tens of nanometers each, while in the case of $Mg_{80}Cu_{10}Y_{10}$ the size of these spheres is almost an order of magnitude larger.

TEM bright field images of the melt-spun specimens together with their respective selected area diffraction patterns are shown in Fig. 6a and b. Figure 6a refers to $Mg_{80}Cu_{15}Y_5$ and Fig. 6b refers to $Mg_{80}Cu_{10}Y_{10}$. Figure 7a and b present HRTEM images of $Mg_{80}Cu_{15}Y_5$ and $Mg_{80}Cu_{10}Y_{10}$, respectively. It can be seen from Fig. 6a that the specimen contains nano-grains. A good estimation of their size can be obtained by looking at the dark grains that are tilted into the zone axes. They are the same size as those detected by the HRSEM. The ring diffraction pattern is typical for nano-grained material, the phase of which was found to be $Mg_2Cu$. As for the $Mg_{80}Cu_{10}Y_{10}$, it can be seen from Fig. 6b that the whole area shown is probably one Mg grain, the diffraction pattern of which is given in the figure.

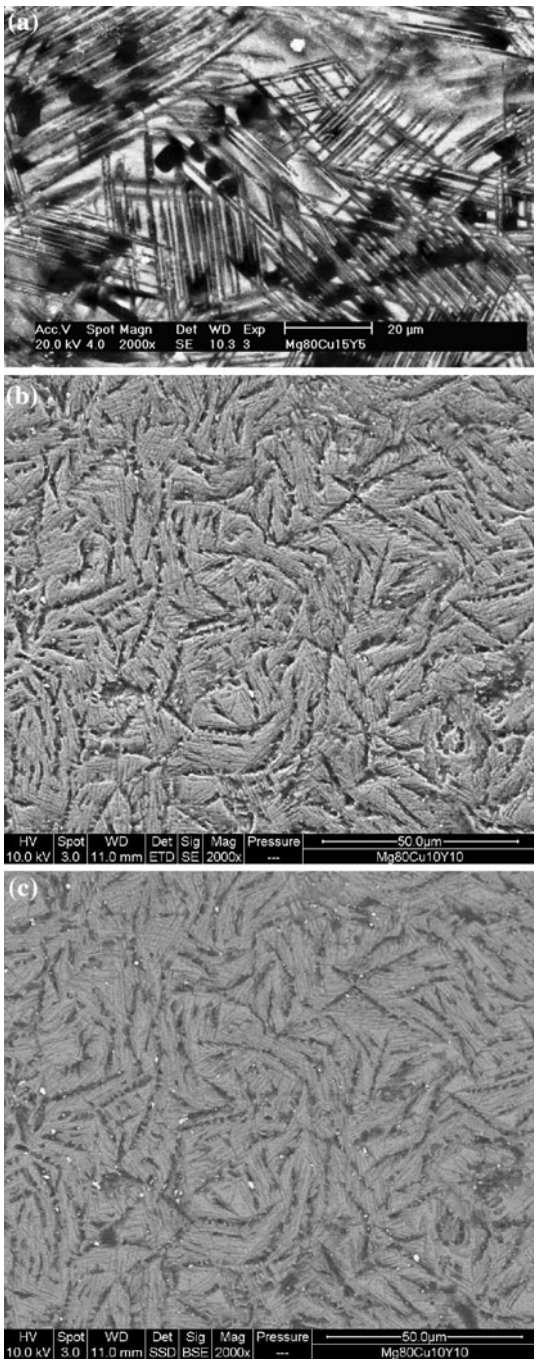


**Fig. 3** SEM micrograph of the gravity casting, mold held at RT: **a** $Mg_{80}Cu_{15}Y_5$ SE, **b** $Mg_{80}Cu_{10}Y_{10}$ SE, **c** $Mg_{80}Cu_{10}Y_{10}$ BSE

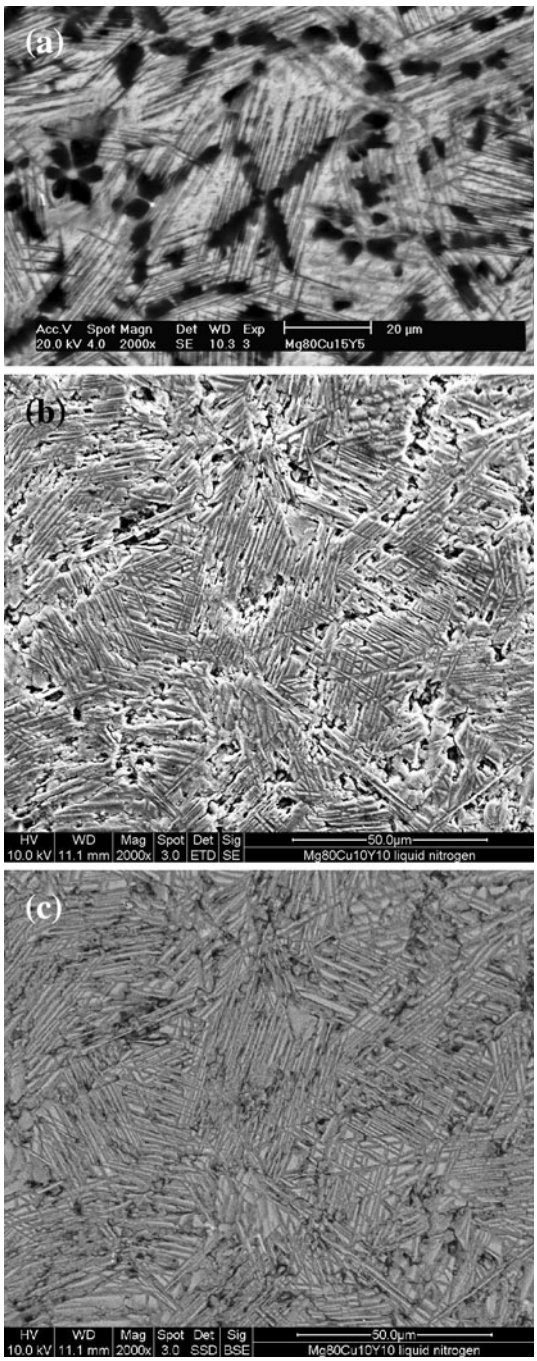


**Fig. 4** SEM micrograph of the gravity casting, mold held at held at −195 °C: **a** $Mg_{80}Cu_{15}Y_5$ SE, **b** $Mg_{80}Cu_{10}Y_{10}$ SE, **c** $Mg_{80}Cu_{10}Y_{10}$ BSE

The high resolution image appearing in Fig. 7a clearly shows a nanocrystalline structure. A few grains having different lattice orientation are discernible. Figure 7b, on the contrary, shows one Mg grain of the $Mg_{80}Cu_{10}Y_{10}$ with its respective FFT. It appears that the average grain size of the $Mg_{80}Cu_{10}Y_{10}$ is a few times coarser than the one of the $Mg_{80}Cu_{15}Y_5$. This finding is in line with the HRSEM images.

## Discussion

As stated earlier, the only XRD pattern showing evidence of amorphous structure is that of the $Mg_{80}Cu_{15}Y_5$ melt-spun specimen and to some extent, the $Mg_{80}Cu_{10}Y_{10}$ melt-one. The XRD analysis of spectra 1–3 of the $Mg_{80}Cu_{15}Y_5$ specimens has already been published elsewhere [16]. It is only necessary to mention that Mg and $Mg_2Cu$ peaks were

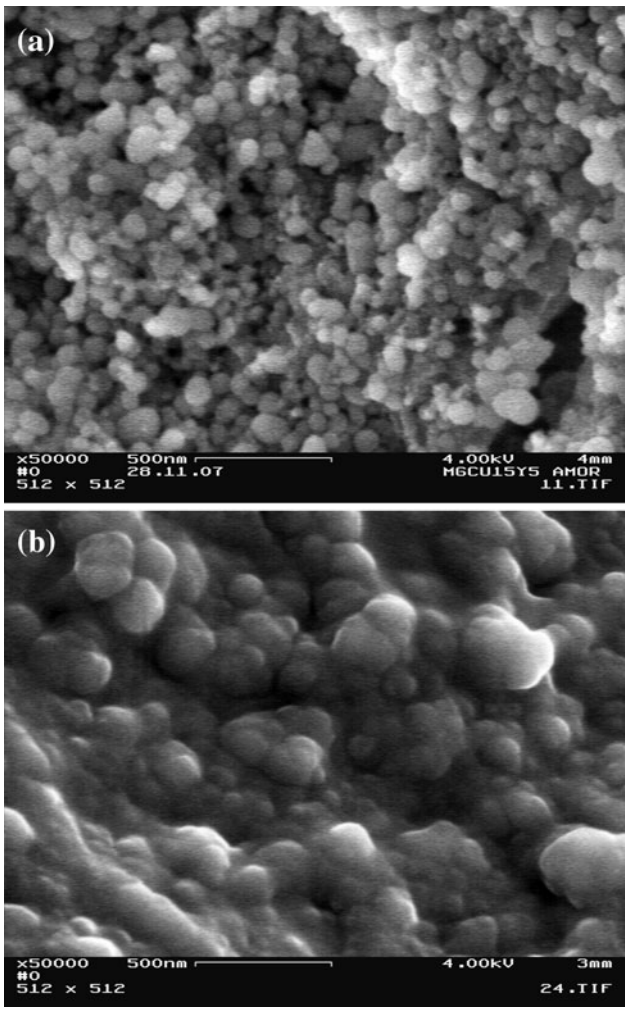


**Fig. 5** HRSEM micrographs of the specimen cast by melt spinning: **a** $Mg_{80}Cu_{15}Y_5$, **b** $Mg_{80}Cu_{10}Y_{10}$

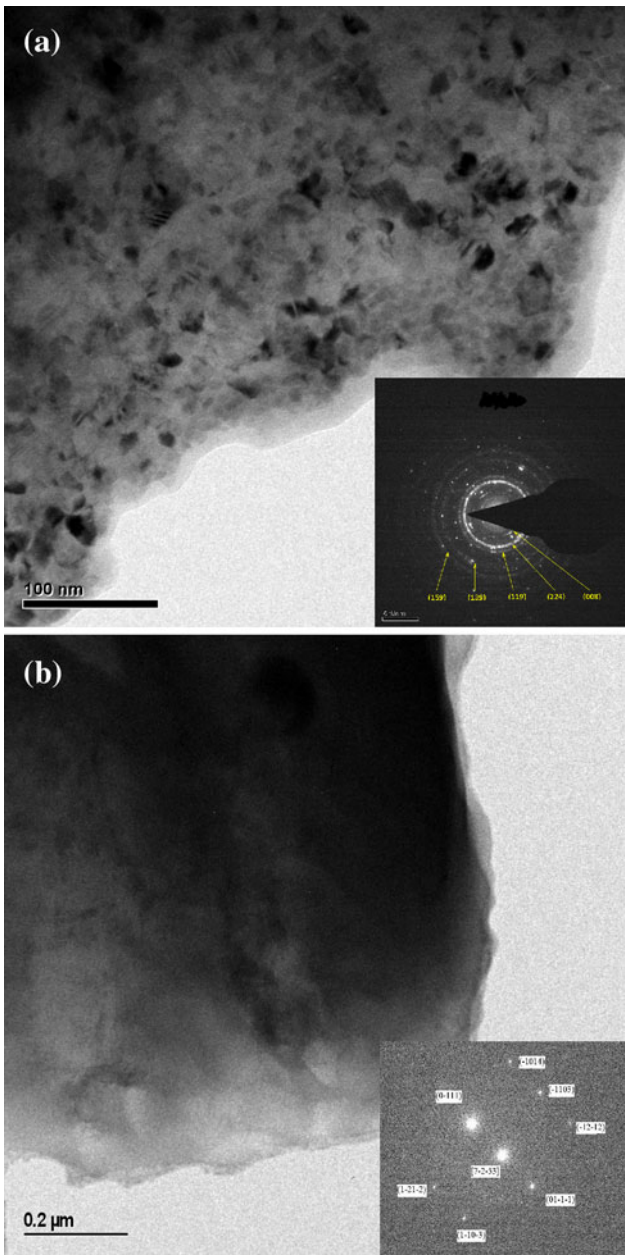


**Fig. 6** TEM micrographs of the specimen cast by melt spinning: **a** $Mg_{80}Cu_{15}Y_5$, **b** $Mg_{80}Cu_{10}Y_{10}$

identified in all cases whereas no reflections of free Y were detected, possibly due to its small volume fraction. However, Mg and $Mg_2Cu$ reflections are slightly shifted to lower angles (higher d-spacings), possibly due to the existence of dissolved Y [16]. It seems that the same analysis is valid in the case of the crystalline $Mg_{80}Cu_{10}Y_{10}$ spectra as well.

It can be seen from the Mg–Cu phase diagram [18] that with a Cu content of either 10 or 15 at.%, both Mg and $Mg_2Cu$ co-exist at RT under equilibrium conditions. As for the Mg–Y phase diagram [18], the maximum Y content does not exceed 1.5 at.% at 400 °C and the maximum solubility limit is even lower at RT. The Y is, therefore, expected to appear in an Mg solid solution and in either $Mg_{24}Y_5$ or $Mg_5Y_2$ intermetallics in both cases of $Mg_{80}Cu_{15}Y_5$ and $Mg_{80}Cu_{10}Y_{10}$.

A detailed SEM analysis of the different $Mg_{80}Cu_{15}Y_5$ gravity-cast specimens has been published elsewhere by the authors [16]. This analysis of the gravity-cast $Mg_{80}Cu_{15}Y_5$ took the limitations of EDS into account together with the XRD results and the phase diagrams [18]. The bottom line of the above analysis is that the microstructure of the gravity-cast $Mg_{80}Cu_{15}Y_5$ specimens shown in Figs. 2a, 3a, and 4a consists mostly of an acicular or a feather-like structure, and concomitantly, the higher the cooling rate, the finer the structure. Darker regions within the acicular structure were found to be Mg with about 4 at.% Cu and 3 at.% Y while the bright particles discernible are non-dissolved Y. In the case

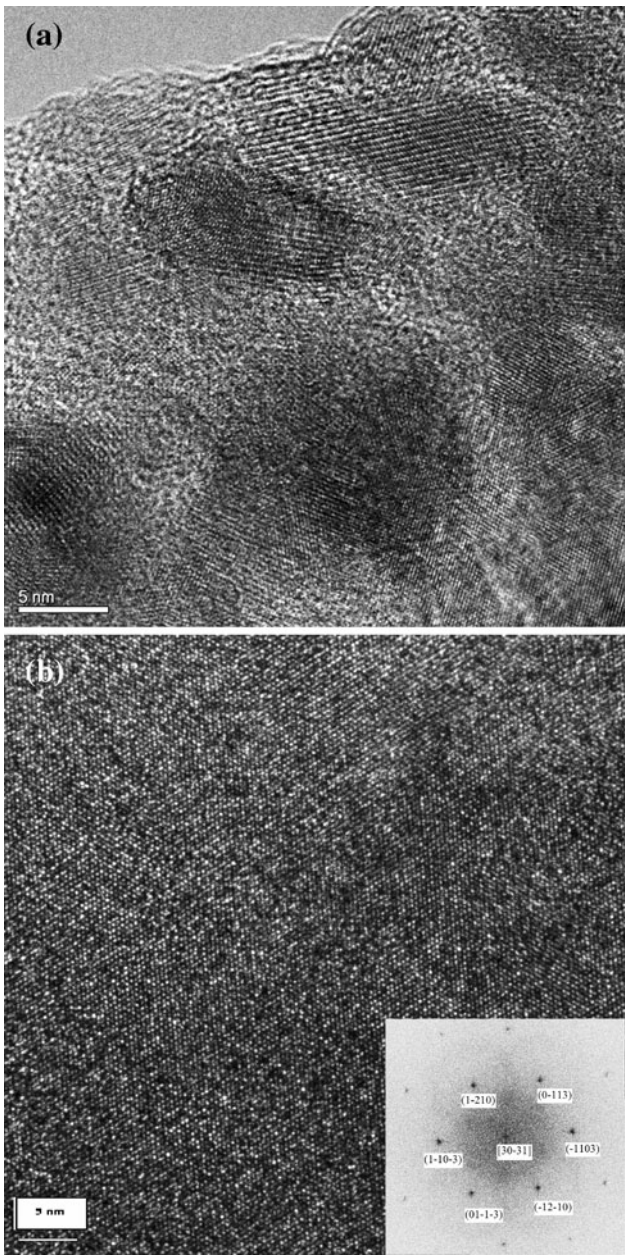


**Fig. 7** HRTEM micrograph of the specimen cast by melt spinning: **a** $Mg_{80}Cu_{15}Y_5$, **b** $Mg_{80}Cu_{10}Y_{10}$

of $Mg_{80}Cu_{10}Y_{10}$ the morphology is similar: namely, acicular or a feather-like but finer than that of $Mg_{80}Cu_{15}Y_5$, which can be seen when comparing Figs. 2a, 3a, and 4a to Figs. 2b, 3b, and 4b, respectively. As stated earlier, no reliable quantitative EDS analysis could be performed on the gravity-cast $Mg_{80}Cu_{10}Y_{10}$ specimens due to the fineness of the microstructure. However, the BSE electron contrast (Figs. 2c, 3c, and 4c) together with the XRD results and the identification of the expected phases according to the Mg–Cu and the Mg–Y diagrams [18] support the claim that the same phases existing in the $Mg_{80}Cu_{15}Y_5$ specimens exist in the $Mg_{80}Cu_{10}Y_{10}$ specimens as well.

As noted above, an XRD spectrum typical for an amorphous material was obtained only in the case of the melt-spun specimens. However, the electron SADP of the $Mg_{80}Cu_{15}Y_5$ (Fig. 6a), with its rings composed of many sharp spots instead of broad diffraction halos, shows evidence of the material being crystalline. The indexed ring diffraction pattern is of $Mg_2Cu$ which is expected to exist according to the Mg–Cu phase diagram [18]. Clear evidence for the crystallinity of the material is obtained from the HRTEM image (Fig. 7a) in which different grains are discernible and the different orientations of adjacent grains can be clearly observed. In the case of the $Mg_{80}Cu_{10}Y_{10}$ it can be seen from Fig. 7b that the specimen is completely crystalline. The respective indexed FFT given in Fig. 7b corresponds to crystalline Mg.

It is well known that when XRD peak broadening occurs it may be difficult to determine whether this broadening arises from the presence of very small, randomly oriented fragments of bulk crystal or from the existence of an amorphous structure. This point was discussed by Spaepen [19] and one example of this issue given in the literature [17] related to $Pd_{75}Si_{25}$. There the average crystal size is of the order of 2 nm. The authors claimed, as published elsewhere [16] that the $Mg_{80}Cu_{15}Y_5$ melt-spun specimen is nanocrystalline and the amorphous XRD pattern obtained originated from the large contribution of the grain boundaries. One may estimate this contribution by assuming that the grains are spherical with an average size of about 30 nm (not far from reality, as can be seen in Fig. 5) that the width of the grain boundary region is about 5 nm (10–15 times the magnesium lattice parameter). It turns out that, under these assumptions, the volume fraction of the grain boundaries is about 70%. It should be noted that estimating the grain size of the melt-spun specimens from the XRD pattern yields finer grains, these discrepancies can be related to the influence of internal stresses on the XRD pattern, namely, peak broadening due to internal stress.

Here it was found that $Mg_{80}Cu_{10}Y_{10}$ was completely crystalline. The XRD peak broadening shown in Fig. 1b can be related to grain refinement. Its higher degree of crystallinity compared to the $Mg_{80}Cu_{15}Y_5$, however, should be discussed. Taking into consideration that the Y does not or almost does not dissolve in the alloy, it seems that chemical composition calculations should be based on the Mg and Cu content without taking the Y into account. In other words, the Mg and the Cu content should be normalized by 0.95 in the case of $Mg_{80}Cu_{15}Y_5$ and by 0.9 in the case of $Mg_{80}Cu_{10}Y_{10}$. Doing this, one can see that the corrected Cu content of the $Mg_{80}Cu_{15}Y_5$ specimen is closer to the eutectic point at 14.5 at.% than that of $Mg_{80}Cu_{10}Y_{10}$. Referring to the semi-empirical rules for producing BMG mentioned in the introduction, it seems that the proximity to deep eutectic is the only discriminating

factor between the two compositions used for the current study.

Spaepen and Turnbull [20] referred to the influence of deep eutectic; they theorized that nucleation and growth are competing amorphizations even under rapid quenching. They concluded that the likelihood of quenching a melt to a glass at a given cooling rate and specimen size will increase with the growth of the ratio $T_g/T_l$ where $T_g$ is the melt-glass transition temperature and $T_l$ is the liquidus temperature. They showed that when $T_g/T_l$ changes from 2/3 to 1/2, the minimum quench rates required to effectively suppress homogeneous nucleation rises by six orders of magnitude. This rise, in turn, explains the importance of choosing compositions close to deep eutectics. However, the growth factor must not be neglected. Spaepen and Turnbull [20] stated that even if nucleation is completely suppressed, crystallization may still occur by growth from heterogeneous nuclei that are usually present unintentionally. Therefore, the formation and persistence of a metallic glass require conditions such that the crystal growth rate in the amorphous metal does not become large enough to effect crystallization from these nuclei. Looking at Fig. 5a and b, the average sphere size in the case of $Mg_{80}Cu_{15}Y_5$ can be taken as 30 nm while in the case of $Mg_{80}Cu_{10}Y_{10}$ the size of these spheres is about 200 nm. This means, in turn, that the number of nucleation events that occurred in the $Mg_{80}Cu_{15}Y_5$ was about $7.1 \times 10^{16}$ $cm^{-3}$ while the number of nucleation events that occurred in the $Mg_{80}Cu_{10}Y_{10}$ was about $2.39 \times 10^{14}$ $cm^{-3}$.

Looking at the Mg–Cu phase diagram [18] one can see that according to Spaepen and Turnbull, the frequency of the nucleation events should have been higher for $Mg_{80}Cu_{10}Y_{10}$ than for $Mg_{80}Cu_{10}Y_5$ due to the respective liquidus temperature being higher. In other words, the appearance of coarser grains in the case of $Mg_{80}Cu_{10}Y_{10}$ seems to contradict the analysis of Spaepen and Turnbull [20]. Spaepen and Turnbull [20] claimed that the amorphization/nucleation competition yields amorphization provided that nucleation rate is suppressed enough. The above results, in opposition, show evidence for the occurrence of massive nucleation in the vicinity of a deep eutectic. This massive nucleation led to the appearance of a large amount of ultra-fine grains, and therefore, an extremely high volume-fraction of crystallographically disordered grain boundaries. In the authors' opinion, further research work will be needed to fully understand the kinetics of the processes involved.

## Conclusions

- The microstructure of $Mg_{80}Cu_{15}Y_5$ and $Mg_{80}Cu_{10}Y_{10}$ castings, obtained under four different cooling rates, was investigated and described using XRD, SEM, TEM, and EDS analyses. An XRD spectrum typical for a completely amorphous material was recorded only in the case of the melt-spun $Mg_{80}Cu_{15}Y_5$.
- In all cases of crystalline material, most of the structure consists of an acicular or a feather-like structure, and concomitantly, the higher the cooling rate, the finer the structure. It was also noted that that the microstructure of $Mg_{80}Cu_{10}Y_{10}$ at a given cooling rate is finer than that of the $Mg_{80}Cu_{15}Y_5$ under the same cooling rate. The phases identified were Mg and $Mg_2Cu$ while Y was detected both as non-dissolved particles and in a supersaturated Mg solid solution.
- TEM study and SADP of the melt-spun specimens revealed a crystalline structure. This finding was supported by HRTEM. HRSEM images revealed that the structure consists of fine spheres, each a few tens of nanometers in size in the case of $Mg_{80}Cu_{15}Y_5$. In the case of $Mg_{80}Cu_{10}Y_{10}$ these spheres were found to be an order of magnitude coarser.
- The size and the number of the observed spherical grains could not be explained on the basis of the frequency of nucleation events.
- Further research work is required in order to understand the kinetics of the solidification/glass transition processes involved.

**Acknowledgements** The authors wish to thank Dr. Y. Kauffmann and Ms. Mor Baram for their assistance with the TEM study; thanks are also due to Mr. S. Avraham for TEM specimen preparation.

## References

1. Hong JW, Kang HS, Yoon WY, Lee SM (2007) Mater Sci Eng A 449–451:727
2. Schlorke N, Weiss B, Eckert J, Schultz L (1999) Nanostruct Mater 12:127
3. Puech S, Blandin JJ, Soubeyoux JL (2007) Adv Eng Mater 9:764
4. Kim D, Lee BL, Kim NJ (2005) Scripta Mater 52:969
5. Pryds N, Eldrup M, Schrøder Pedersen A (2001) In: Proceedings of the 22nd Risø innernational symposium on materials science: science of metastable and nanocrystalline alloys structure, properties and modeling, Risø National Laboratory, Roskilde, Denmark, pp 377–382
6. Savyak M, Hirnyj S, Bauer HD, Uhlemann M, Eckert J, Schultz L, Gebert A (2004) J Alloys Compd 364:229
7. Satta M, Palumbo M, Rizzi P, Baricco M (2007) Adv Eng Mater 9:475
8. Inoue A, Masumoto T (1993) Mater Sci Eng A 173:1
9. Inoue A, Nakamura T, Nishiyama N, Masumoto T (1992) Mater Trans JIM 10:937
10. Inoue A, Kato A, Zhang T, Kim SG, Masumoto T (1991) Mater Trans JIM 32:609
11. Wolff U, Pryds N, Wert JA (2004) Scripta Mater 50:1385
12. Chen G, Ferry M (2007) J Mater Sci 42:646. doi: 10.1007/s10853-006-1140-2
13. Kim SG, Inoue A, Masumoto T (1990) Mater Trans JIM 31:929

14. Murty BS, Hono K (2000) Mater Trans JIM 41:1538
15. Ma H, Zheng Q, Xu J, Li Y, Ma E (2005) J Mater Res 20:2252
16. Katz A, Rosenson H, Koren Z, Regev M (2009) Mater Sci Technol 25:1227
17. Davis JR, Allen P (1990) ASM handbook, 10th edn. ASM, USA
18. Massalski TD (1987) Binary alloy phase diagrams, 2nd printing. ASM, USA
19. Spaepen F (1989) Mater Res Soc Symp 132:127
20. Spaepen F, Turnbull D (1976) In: Grant NJ, Giessen BC (eds) Proceedings of the second international conference on rapidly-quenched metals. The Massachusetts Institute of Technology, Cambridge, USA, p 205